A UAV Based System for Real-Time Near-Infrared Monitoring of Small-Scale Wildfires

Edwin Magidimisha
Optronic Sensor Systems, Defence and Security,
Council for Scientific and Industrial Research
Pretoria, South Africa
e-mail: emagidimisha@csir.co.za

Seelen Naidoo
e-mail: snaidoo7@csir.co.za

Zimbini Faniso-Mnyaka
e-mail:zfaniso@csir.co.za

Muhammad Ahmed Nana
e-mail: mnana@csir.co.za

Shrikant Virendra Naidoo
e-mail: svnaidoo@csir.co.za

Vusi Skosana
e-mail: vskosana@csir.co.za

***Abstract*—Wildfires are a global threat that is becoming more severe and widespread due to climate change. These fires not only pose a significant risk to human life, firefighters, and infrastructure, but also endanger forest resources, increase greenhouse gas emissions, and cause huge economic losses. Several researchers have been working to find dedicated solutions for early wildfire detection, tracking, and firefighting assistance. Traditional methods of fire detection have mainly been from fire lookouts in towers, infrared sensors on elevated platforms, surveillance of fires from aircraft, and remote sensing from satellites. Although these techniques have been proven to work in other areas, they are unsuitable or are limited in performance due to various reasons, e.g., human accuracy, sensor field of view limiting coverage to smaller areas, sensor cost-effectiveness, and re-visit time on a satellite. To counteract the problem, a real-time wildfire monitoring system that can detect small-scale wildfire events and that can be used for tactical forest firefighting operations is proposed. The concept takes advantage of vegetation biomass combustion by-products such as the alkali element Potassium (K) that is emitted at the flaming phase of the fire. The technique is specific to the flaming phase of the fire and is not affected by the fire size. It employs two high-resolution, cost-effective complementary metal-oxide-semiconductors (CMOS) with high quantum efficiency within the near-infrared (NIR) spectrum. The sensor uses ultra-narrow-band filtering and target-to-background rationing techniques for the detection of vegetation fires. The system is designed to be self-contained, having its supporting power, compact, and lightweight for easy integration on different types and sizes of unmanned aerial vehicles (UAV) to provide real-time detection and support to firefighters while airborne. UAVs can provide a low-cost alternative for the reduction of fire disasters through early detection, reporting, and real-time support for firefighters. This paper presents the experimental results of an NIR optical sensor mounted on a UAV carrier that was used to collect data while flying at low to 200m above ground at the Centurion Grassland Flying Club. The results provide evidence of the presence of K in small-scale actively burning vegetation fires observed at different angles and detectable from a UAV. The results support the use of NIR sensor payload for the detection of small-scale fires from a UAV platform.**

Keywords - Climate; CMOS; Near-infrared; Potassium (K); UAV; Wildfires.

I. INTRODUCTION

The fire incidences and severity are expected to increase in response to climate change [1, 2, 3, 4]. Fire prevention, detection, monitoring, and suppression of wildland vegetation are key economic and public safety concerns in many parts of the world [5]. These wildfires further exacerbate climate change due to CO_2 and black aerosol emissions. This serves as a strong motivation for the development of an optical surveillance system that can detect and monitor wildfires on a small scale. Classical remote sensing of vegetation fires has been through the detection of Planckian emission in the medium wave infrared (3-5 µm, MWIR) and the long-wave infrared (LWIR) band of the electromagnetic spectrum [6,7,8]. The short wave (1 – 2.5µm, SWIR) infrared band was exploited and deployed on the Airborne Visible Infrared Imaging Spectrometer (AVIRIS) platform [9] for the detection of wildfires. IR-based systems, whether cooled or uncooled, can be costly and significantly affected by other heat-emitting sources, leading to clutter or false alarms [10].

With the advancements in passive imaging sensors and filter technologies, reliable commercial-off-the-shelf (COTS) products are now available and more affordable. New sensor technologies such as high-resolution charge-coupled device (CCD) and complementary metal-oxide-semiconductor (CMOS) sensors provide an opportunity to enhance wildfire detection, monitoring, and reporting. As an alternative to other fire detection techniques, this study proposes the use of a compact and cost-effective system for the detection of wildland vegetation fires by observation of the Potassium (K) spectral line. An initial concept study was performed to characterise the various vegetation species inside and outside the laboratory at the Council for Scientific and Industrial Research (CSIR) campus in Pretoria [11]. The study was made to ensure the relevance of the concept to local conditions by investigating the use of atomic lines emission lines in

burning South African vegetation. Vegetation plant species contain a series of trace elements (Na, K, Mg) that present unique narrowband spectral emission lines in the visible and near-infrared (NIR) wavelength range when biomass is heated to high temperatures during the combustion process [12]. Potassium spectral lines can be discriminated against any other background by detector systems that are less costly than the longer wavelength, actively cooled instruments most used in Earth Observation (EO) systems [12]. The K spectral line doublet located within the NIR at 766.5 and 769.9 nm is of particular interest for this application [10,17,19,20]. The current study integrates the NIR optical payload and operates it from an unmanned aerial vehicle (UAV) using remote sensing techniques.

II. BACKGROUND

In recent years, we have seen great progress in the use of UAVs with advanced software for forest fire monitoring, detection, and firefighting. Integration of UAVs with remote sensing techniques aims to provide rapid, mobile, low-cost, and powerful solutions for various fire tasks [13]. Firefighting agencies typically use fixed detection platforms such as towers, aerial patrols, and satellite imagery to directly detect forest fires, rather than relying on reports from the public. However, high-elevation platforms are not well suited for area coverage and can result in some areas developing fires unnoticed. Although aircraft are considered efficient in firefighting, they are expensive to keep airborne for constant monitoring. Compared to fixed ground-based wildfire detection systems, UAVs can provide a broader and more accurate perception of fire from above, especially in areas that are inaccessible or considered too dangerous for firefighting crews. During firefighting, UAVs provide eyes from above, operators can use them from a safe place and can provide important information on the progression of the fire.

In [14], a vision-based UAV-mounted system for the detection of forest fires that uses both the motion and the chroma characteristics of the fires was proposed. The two characteristics were used for the decision rules to improve the reliability and accuracy of fire detection. A method to detect forest fires using a UAV equipped with an optical and an infrared (IR) camera has been proposed [15]. The method uses a LAB colour model and a motion-based algorithm, followed by a maximally stable extremal region (MSER) extraction module. For better visualisation, forest fire detections were combined with landscape information and meteorological data. In a study in [16], a convolutional neural network (CNN) model was trained using optical and infrared sensor data to detect smoke and fire.

III. DETECTION PRINCIPLE

A simplified schematic of the fire detection principle is shown in Figure 1. The figure illustrates a comprehensive outline of the fire detection system and the principle of operation. The principle relies on the abundant nature of Potassium element in vegetation species. The system incorporates a dual camera to capture and record images of burning biomass fires, specifically vegetation fires containing the Potassium element radiometric signature. One of the sensors is optimized for the detection of the K-line and the other for the detection of the background. The captured images are processed using the in-house developed CSIR algorithm applied during the image processing stage to analyse the pair of images and establish whether a fire has been detected.

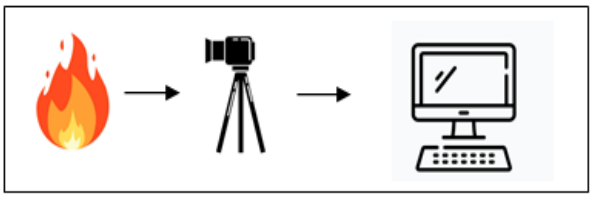

Figure 1: Simplified schematic depicting the overview of the fire detection system.

A. The Potassium Element

Potassium belongs to the alkali metal group and is in the first column of the periodic table. It is one of the most abundant elements in vegetation species [17, 18]. It has a single valence electron that presents unique narrowband spectral emission lines within the visible and NIR wavelength range when biomass is heated to high temperatures in the flaming phase of the fire [19]. The spectral emission of K appears as a doublet at the 766.5 nm and 769.9 nm spectral bands [20]. With advances in optical filter design, filters can now detect low-level signals while suppressing almost all emissions within the outer band by targeting specific elemental emissions from a source signature. These advances in technology open the door for the development of compact sensors capable of detecting narrow spectral lines that can be advanced to compete with other passive sensors operating in other bands. In this study, ultra-narrow band imaging is used for the detection of K using CMOS detectors. The integration of COTS, and ultra-narrow band imaging allows the design of compact and less power-hungry systems, which can be easily integrated on a weight, size, and energy-constrained UAV platform. The CSIR-designed payload weighs 1.8 kg including power support.

B. Fire detection system

A detailed description of the current and futuristic practices in the context of fire detection and monitoring strategies is described in a review paper by F. Khan et al. [21]. Traditional fire detection mechanisms have been through thermal sensors, but other researchers are developing other methods to improve the detection and monitoring of fires for both indoor and outdoor conditions. There are also two broad approaches to fire detection algorithms. The first is using machine learning, which is still in its early stages. The second is to use colour, form, flicker frequency, and the dynamic structure of fire. The fire detection method presented here would fall in the second category. Using radiometric

principles to separate the background from the target (fire) the aspiration is to have a very low false positive rate.

The NIR fire detection sensor presented in this study is made up of two NIR imaging systems placed side-by-side with a common (overlapping) field of view (FOV). These cameras are fitted with ultranarrow band filters with 1 nm bandwidth sensitivity at 769.9 nm, referred to as the K-line band, and 757 nm, referred to as the reference band. The target and reference channels are temporally synchronised at the electronic level so that pairs of images (one from the K-line and the other from the reference band) are obtained at the same instant. Fires are detected by comparing the K-line channel image with the reference channel image. Pixels that are much brighter in the target channel relative to the reference channel are candidate fire detections.

C. Image processing algorithm

The system's image processing begins after the two images are captured, the image with K-line emission, and the other with the background or reference. The images from the two sensors are captured synchronously. The images are not modified with any image enhancement algorithm and are not compressed to preserve the fire front K-line signal emissions. The reference image is resampled to align with the K-line image pixels. This is done by mapping and using a Lucas-Kanada optical flow algorithm [22]. Sections of the individual images that are not common in both are then cropped out, leaving two images of the exact same scene. The fire detection algorithm is applied to the matched cropped K-line and reference images. Fire detection is done using the image ratio technique [23]. Figure 2 illustrates a block diagram that gives an overview of the algorithm.

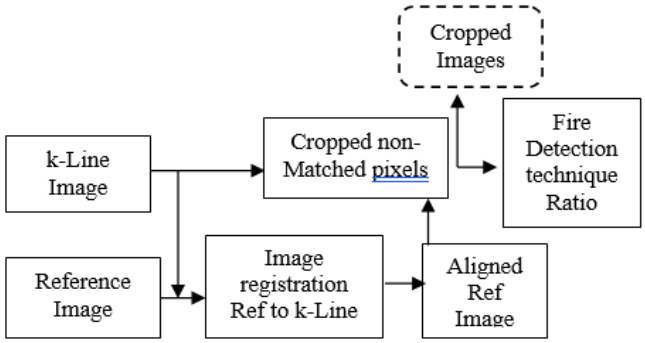

Figure 2: Overview of the K-line fire detection principle.

The K-line and reference images will have the same nominal FOV but will not be pixel-aligned. This is due to the following:

a) The difficulty of perfectly mechanically aligning the optical axes and image plane rotations of the two channels and
b) A possible slight mismatch in the effective focal length (EFL), which means that the two channels will have slightly different image scales and not an exact FOV.
c) Instability of both optical channels due to vibrations during flight.
d) Although the optical systems are identical, there will be minor differences in the image sensor and lens (which need to be corrected).

It may not be possible to rely on a fixed relationship between the pixels of the reference channel and those of the K-line channel from a pre-flight calibration due to the instability from vibrations during flight that could shift the camera's perspectives slightly. Image registration or alignment per image pair is performed in the following way:

a) Feature detection is done by obtaining good features to track as described in [24]. This is done for each image individually, to produce two lists of features.
b) These lists of features are passed to a Lucas-Kanade optical flow algorithm to find and order the features that exist in both images.
c) The features that do not co-exist in both images are pruned and removed from the lists.
d) The perspective transform between the two lists of pruned features is then calculated using the RANSAC method [25, 26].
e) The reference image is then perspectively warped using the previously calculated perspective transforms.

The image ratio technique is simple and is implemented as follows:

a) Compute the ratio image, that is, the K-line image divided by the reference image.

$$im_{Ratio} = im_{kline}/im_{reference}$$

b) Compute the global mean (μ) and variance (σ) of the image ratio.
c) Compute the variant for each pixel in the ratio image as:

$$\sigma_p = \sqrt{(p(i,j) - \mu)^2}$$

where p is at location (i, j).

d) If the variance of a pixel is greater than the global variance multiplied by a user-defined sensitivity integer value i.e., $\sigma_p > k\sigma$,the pixel gets classified as a fire front pixel.
e) Otherwise, the pixel is classified as a non-fire pixel and is discarded.

The result or output of the image ratio technique is a binary mask image that has a value of 1 when fire was detected on that pixel, and a value of 0 when no fire was present. The mask image is then passed onto a simple blob detector [27] to filter out any noise or false detections and automatically indicate when a fire was detected. Automatic flagging is possible since no blobs will be found when there is no fire present.

The entire image processing process was implemented in Python programming language using the OpenCV library.

Processing speed can be trivially improved by using the C++ or CUDA implementations of the OpenCV library.

IV. METHOD

The field measurements test was conducted on the 18th of March 2022 at the Grasslands Flying Club in Pretoria West, South Africa. The purpose of the test was to evaluate the aerial performance of the NIR optical fire detection sensor onboard a UAV. Shown in Figure 3 is a photograph of the NIR imaging sensor system during its lab testing phase.

Figure 3: A closer look at the NIR sensor with two CMOS optical sensors placed side by side and furnished with ultra-narrow filters. A third wide field-of-view visible camera is also inserted and placed above the two cameras.

The UAV Payload uses a development board (Raspberry Pi4 8GB) to control the capturing of images, communication with a ground station, and storage of captured images. The captured images were stored on board a micro-SD card and removed after the completion of a sortie. When the memory card is removed from the payload and the data is retrieved for archival, the data is inspected while the next mission is ongoing. Fire detection is performed on a post-processing basis by automatically analysing the images stored in the memory card.

The basic NIR sensor payload consists of the following components:

- A processor module with storage
- the K-line dual camera system,
- a viewfinder camera,
- a telemetry radio downlink,
- an analog video downlink,
- high-definition video downlink,
- a power source, and
- wiring harnesses.

Figure 4 is a representation of the K-line NIR UAV system and its supporting systems in the operational environment. The list of systems and supporting systems follows with a brief description of the context of a typical operational scenario.

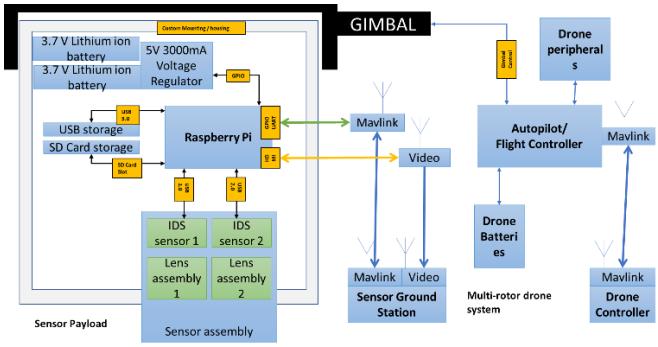

Figure 4: UAV with functional block diagram of the NIR sensor payload

The NIR UAV Payload system (required system) consists of the sensor modules, optics, and processing package in a configuration that accommodates data logging, transmission, and telemetry with the dedicated ground station. The video and telemetry transmission links are separate and isolated from the UAV's communication and control system. The NIR UAV Payload system collectively refers to the physical payload packaging, as well as the ground station and the communication interfacing modules. The use of the system entails the responsibilities of the operator.

The UAV system (supporting system) refers to the UAV airframe (in this instance, a rotary-wing drone) and its gimbal. It includes the UAV pilot's ground station (typically mission planner / ardu pilot). UAV control and gimbal control are designated responsibilities of the UAV pilot. The experiments required coordination between the UAV and payload controller personnel.

The payload system operates in a free-running mode that is triggered by the ground station operator. In the typical context of a fire surveillance exercise for large, restricted areas or where accessibility is challenging, a UAV system is ideal for creating situational awareness of the fire and its spread. The intended mode of operation is illustrated in Figure 5.

The processing module posed significant limitations when implementing onboard processing, making the effective framerate unusable. More limiting was the thermal impact of processing onboard with the processor exceeding its rated threshold. For this reason, the ground station triggered a recording of relevant data, captured to the storage device. Upon the UAV's return to the ground station, the captured data was manually retrieved and post-processed on the ground station system. The video transmission modules were not reliable enough to transmit processable data during flight, hence the decision was taken to post-process data in between each flight path cycle which for the DJI 600 drone was limited to 30 minutes.

A UAV-licensed groundskeeper was tasked to pilot the UAV into a strategic position to capture visual data regarding the fire. The ground station controller has access to trigger the various operational modes of the system. This iteration can

trigger free running record modes, swap between video transmission feeds, and provide general status feedback and control during the flight path. The state mode model of the system is illustrated below.

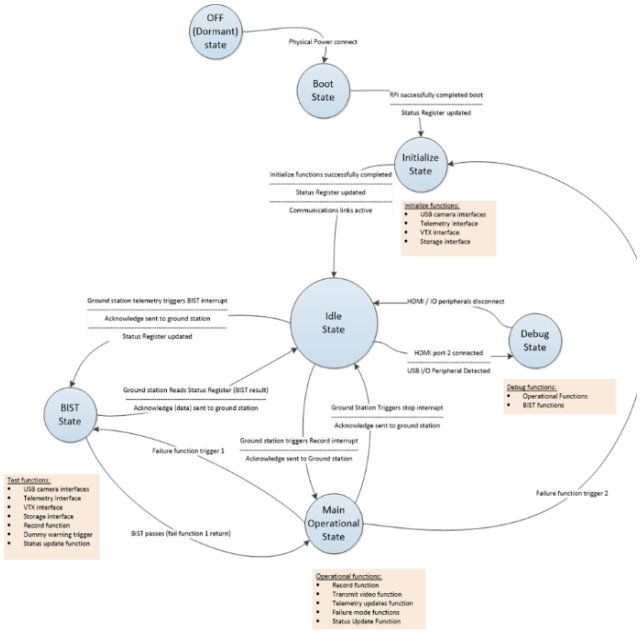

Figure 5: Modes of operation for payload

Shown in Figure 6 is the NIR fire detection payload onboard the UAV taken during the deployment experiment at the Grasslands Flying Club.

Figure 6: UAV with NIR sensor payload on the DJI 600 drone during a field fire detection test of the sensor.

Several sorties were carried out during deployment to test the new NIR payload aboard an airborne UAV. The purpose of the test was to determine whether the new NIR sensor can detect ground wildfires from the air at relatively low altitudes (approximately 200 m above ground level) and at different aspect angles from the fire. The size of the fire on the ground was approximately 500 cm by 500 cm.

The UAV and the Payload systems are completely isolated with respect to power distribution and telecommunications, with the Payload system including its own battery and independent telemetry transceivers. The UAV employs a proprietary gimbal (3 degrees of Freedom) with a manual rotary clamp system. No adhesives, custom mounting brackets, or specialised tools were required for the mechanical coupling of the two systems. The following equipment was used during the test:

- M600 UAV with RONIN gimbal provided and piloted by UAV Industries (UAVI),
- UAV NIR Payload sensor,
- UAV Ground Control Station,
- FieldSpec 3 Max Analytical Spectral Device (ASD) with spectral range 350-2500 nm,
- Weather Station.

A. *Atmospheric Conditions*

During field measurements, the scenario demands that atmospheric computations be made to accommodate the atmospheric effects, caused by molecular absorption and emission (mainly water and CO_2, as well as atmospheric scattering processes by aerosols). Atmospheric modelling codes such as MODTRAN, HITRAN, and others can be used to simulate atmospheric transmission as described below. The radiative transfer is conducted to confirm the detectability of the Potassium lines within the atmosphere.

Atmospheric transmission was calculated using the HITRAN Radiation Transfer Model (RTM) in the NIR region, as shown in Figure 7. The downloaded HITRAN data were on a vacuum scale and converted to air using the Edlen equation (NIST). The following parameters were used: 20°C air temperature, 101325 Pa air pressure, and 50% humidity [18]. The red lines show the K doublet at 766.5 nm and 769.9 nm. The 766.5 nm is absorbed by atmospheric Oxygen (O_2) located at the O_2 absorption line and therefore cannot be detected remotely. The K emission lines are within the range of the sequence of the atmospheric absorption lines that peak at about 762 nm [24].

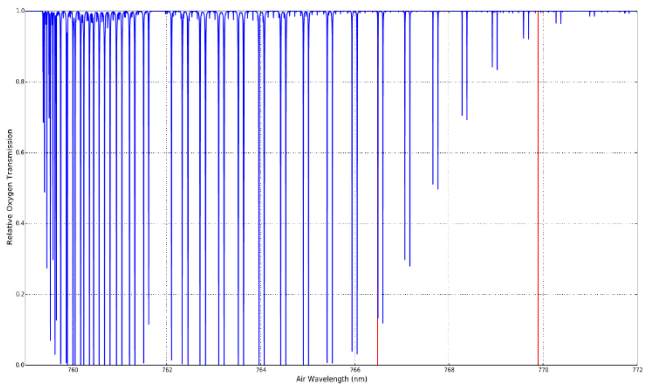

Figure 7: The high spectral resolution Oxygen atmospheric transmittance near the wavelength location of the two Potassium emission spectral lines, data from HiTRAN (http://. iao.ru).

The positions of the K-lines are indicated by two vertical red lines, and the deep lines show the absorption effects arising from the atmospheric Oxygen gas. The filter position choice of 769.9 nm is based on the transmission data above, showing that the 766.5 nm is absorbed by atmospheric Oxygen.

B. Field UAV measurement

The test consisted of a controlled ground fire using wood and dried grass as fuel. An analytical spectral device was placed on the ground close to the fire (approximately 3 m), which was used to record the spectral signature of the fire as it burned. It provided reference spectral data of the fire from the ground to check whether the NIR signature was contained within the fire. The range at which the detection tests were conducted was approximately 200 m (radially) from the fire over various elevation angles with a centered perspective at the burn zone:

- Test point 1: *The elevation angle is 0 degrees, 200 m from the burn zone.*
- Test point 2: *Elevation angle of 45 degrees, 200 m from burn zone.*
- Test point 3: *Elevation angle of 90 degrees (perpendicular to ground level), 200m from the burn zone.*

At these test points, the UAV pilot was unable to maintain rotation orientation (yaw) for data capture due to wind conditions. The position was confirmed through a video stream to the ground station with effort placed in centering the burn zone in the field of view only. The yaw orientation of the sensors had no impact on the detection. These test points provided sufficient data to prove the initial success of the fire detection system. Results are highlighted in Section V. Figure 8 provides an illustrative overview of the mission profile test points used during the fire detection tests.

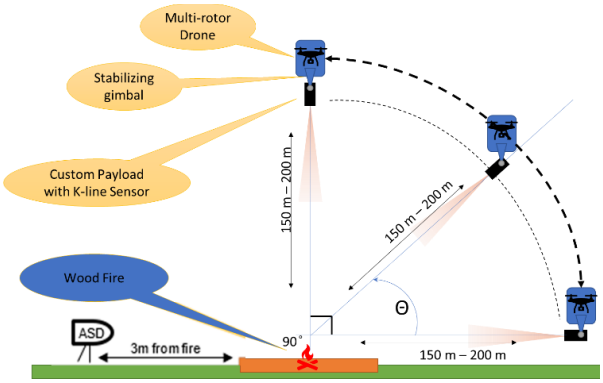

Figure 8: Illustrative overview of flight mission profiles.

C. Hardware Setup

UAV, gimbal and Payload preparations required the UAV operator contractor to provide swappable alternating sets of UAV batteries for the M600 UAV and their control station. The M600 guaranteed a maximum flight time of 30 minutes, of which 20 was allocated to the experiment flight paths, the alternating battery sets allowed for experiment continuity. Similarly, the Payload battery system was designed with two sets of alternating batteries to facilitate the same objective during the experiment. The payload ground station consisted of two laptops in a ruggedized case requiring two operators, viz: a gimbal operator (laptop 1), and a Payload operator (laptop 2). The experimental hardware configuration for the experiment is illustrated in Figure 9 below.

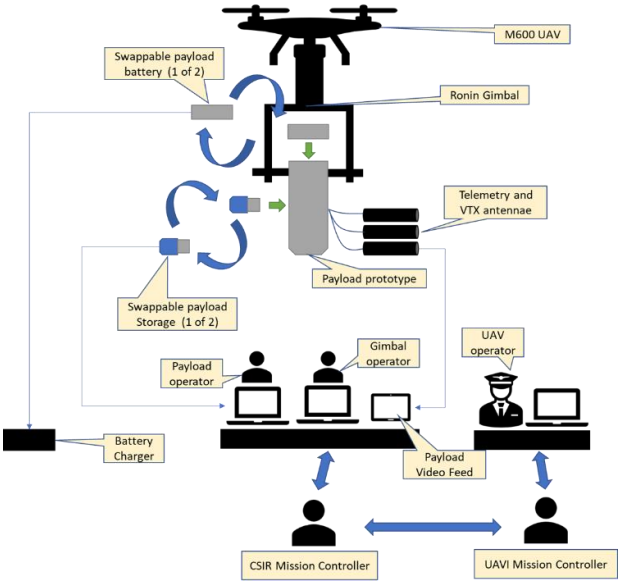

Figure 9: Experimental hardware configuration setup.

V. RESULTS

In this section, the results obtained from the field measurements detection tests, which encompass data collected through both UAV NIR image sensors and spectral measurements recorded by the ASD spectroradiometer, are presented.

A. UAV NIR image sensor data

When examining the results derived from the UAV NIR image sensors, we display them in pairs for clarity. The image on the left represents the masked image, while the image on the right image showcases the target image, which exhibits the distinctive K-line emission signature. Following the application of image processing techniques, the K-line signature is highlighted in red as an overlay, while the black and white target image emphasizes the masking process, effectively isolating the K-line signature.

B. ASD FieldSpec 3 Spectroradiometer Data

The ASD collects a spectrum covering a broad wavelength region (350 nm to 2400 nm) almost instantaneously and has an absolute radiance calibration traceable to NIST. The ASD FieldSpec 3 spectroradiometer data is presented in groups of three images. The top image zooms in on the K-line doublet, offering a detailed view. The image in the middle displays zoomed spectra of several instances of the fire captured at different times, the third figure is a complete spectral image of the fire across the 350-2500 nm spectral band. In these figures, the emission spectrum of the fire becomes prominently visible, with the spectral radiance generally increasing with wavelength. It is clear from the results that the resolution of the ASD is too low and was unable to resolve the K-line doublet.

For this deployment, we conducted controlled burns of dried grass to capture both NIR images from the UAV and spectroradiometer data from the ASD FieldSpec 3. These results contribute to a comprehensive understanding of fire detection mechanisms, spectral signatures, and atomic compositions. Various flight profiles were flown to test the sensor performance at different angles as shared below.

C. Test Point 1:0 Degree Aspect Angle Fire Detection

The image below shows the setup of the NIR imaging sensor at zero degrees relative to the fire.

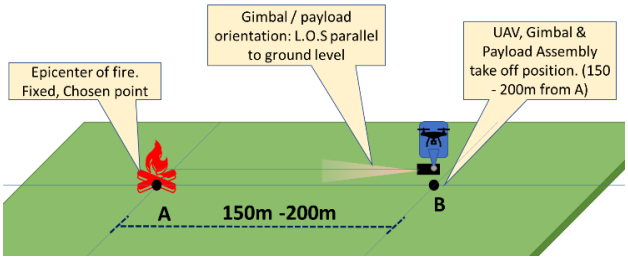

Figure 10: Illustration of the drone viewing the fire at 0 degrees.

The sensor was able to detect fire from an angle (in this scenario, the angle 0° is used). The images were captured while the drone was at 0°, as shown in the image Figure 10.

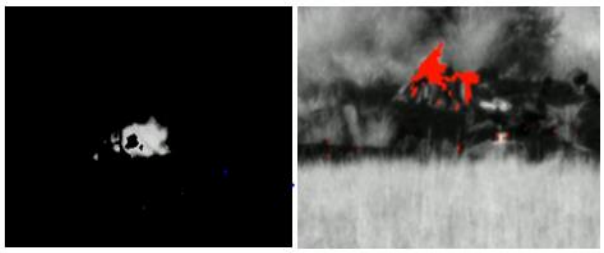

(a) (b)

Figure 11: NIR sensor images during the lower angle of 0 degrees detection.

The sensor images are as shown above. On Figure 11(a), is the masked image and on the right, Figure 11(b) is the detection image showing the K-line detections in red.

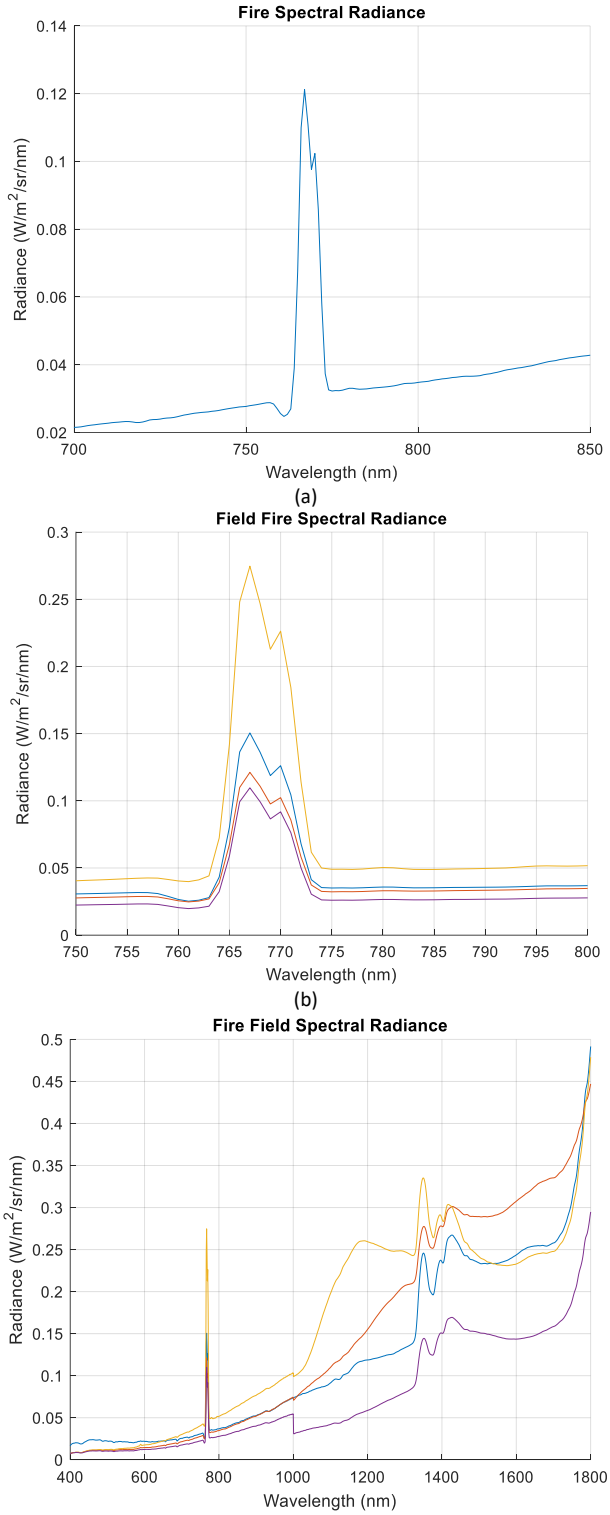

Figure 12: ASD spectral data with NIR-zoomed K-line doublet (a) and (b) and (c) is the full spectral set of the measurements. The Figure shows the spectral radiance of the fire within the NIR region.

The NIR signature was successfully detected in its entirety by the ASD spectral sensor, strategically placed near the fire

scene. The corresponding ASD data is presented in Figure 12. Throughout the airborne operation, multiple spectral measurements were meticulously collected, as visually illustrated in Figures 12(a), Figure 12(b), and Figure 12(c). A similar kind of information is shown in Figure 15 and Figure 18.

D. Test Point 2:45 Degree Aspect Angle Fire Detection

Figure 13 shows the UAV carrying the NIR sensor payload at 45 degrees from the fire.

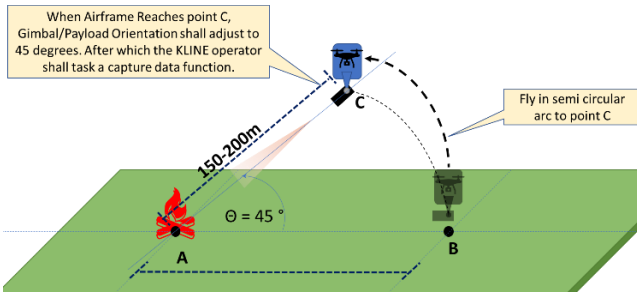

Figure 13: Illustration of the UAV sensor at a 45-degree aspect angle

The sensor demonstrated the ability to detect fires from an oblique angle, specifically at 45 degrees in this scenario. Images were acquired during the drone's operation at a 45° angle, as visually depicted in Figure 14. In Figure 14(a), we present the masked image that highlights the K-line emission originating from the fire. Meanwhile, Figure 14(b) presents the unmasked image, with the K-line emission accurately delineated in red for enhanced visibility.

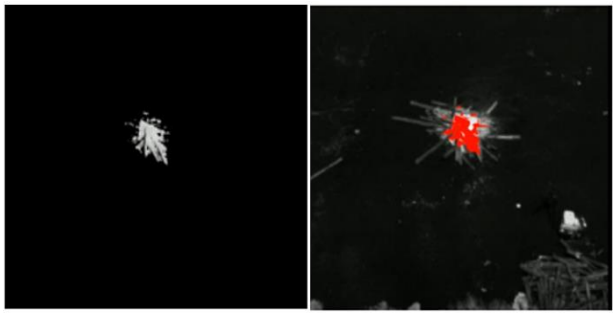

(a) (b)

Figure 14: NIR sensor images during angular (45 degrees) fire detection.

The ASD spectral sensor was strategically positioned near the fire scene, to characterize the flaming vegetation fire spectrally and effectively within the NIR region. While the UAV was in flight or airborne, we conducted multiple ASD spectral measurements, which are illustrated in Figures 15(a), Figure15(b), and Figure 15(c). In particular, Figure 15(a) offers a close-up view of the spectra, highlighting the unresolved K-line doublet, a consequence of the ASD's modest resolution of 3nm.

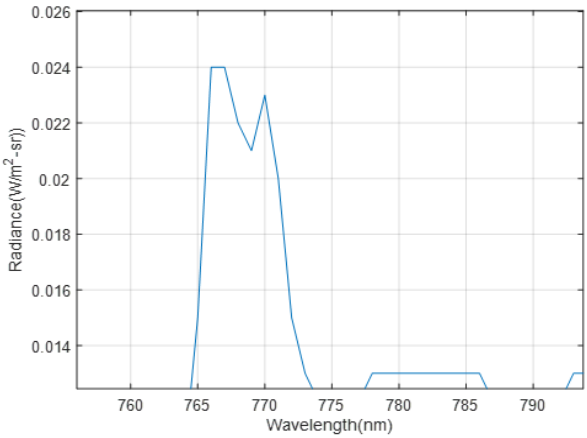

(a)

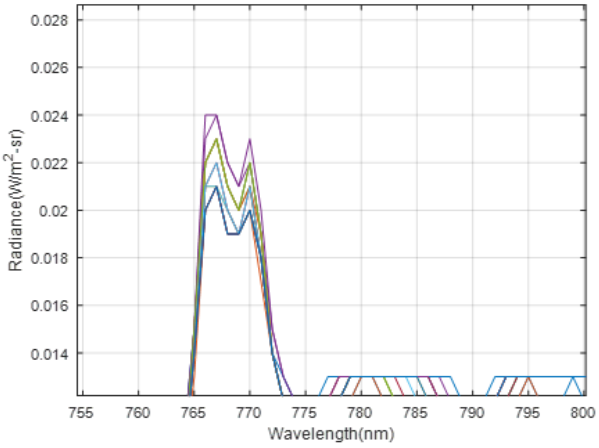

(b)

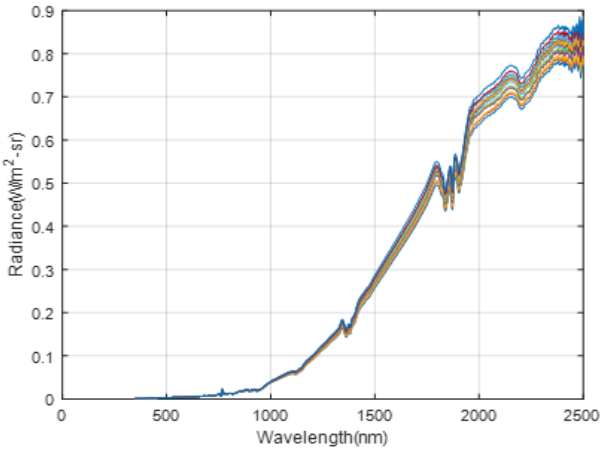

(c)

Figure 15: ASD spectral data with NIR-zoomed K-line unresolved doublet. The fire shows the spectral radiance of the fire within the NIR region.

The full fire spectrum was taken at various instances during the fire progression and it shows an unzoomed K-line presence at 769.9 nm. Visible is the continuous background black body spectrum that rises rapidly with increasing

wavelength. This is purely due to the thermal excitation of all atomic and molecular species within the flaming region. Provided that the fire was flaming (as opposed to smoldering), the burning vegetation within the FOV of the ASD, the K-line doublet was readily evident in the collected spectra.

E. Test Point 3: Flying directly above the fire (90 degrees aspect angle)

Figure 16 shows the UAV carrying the NIR sensor payload at a 90-degree aspect angle from the fire.

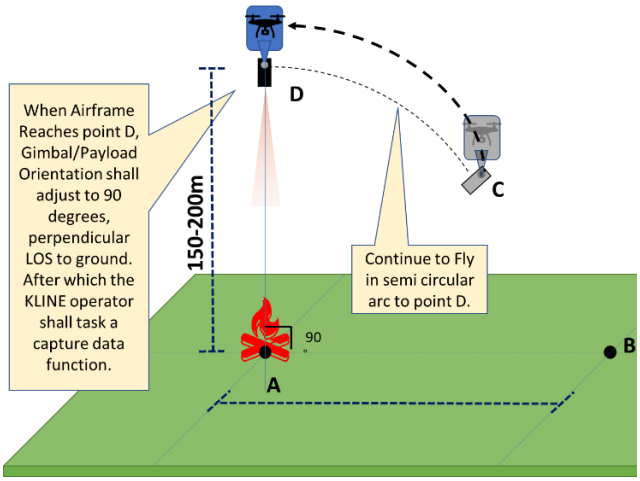

Figure 16: Image depicting the flight path of the UAV from point C TO point D above the fire.

The sensor was able to detect from directly above, as shown in Figure 17. The figure shows the NIR images detected by the K-line band.

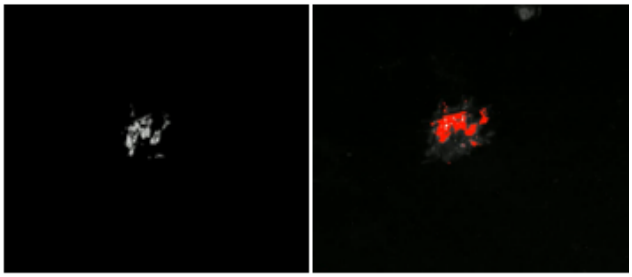

(a) (b)

Figure 17: NIR sensor images showing fire detection from directly above (90 degrees).

Successfully data logging was achieved with the ASD sensor, as depicted in Figure 18. Shown in Figure 18(a) are the zoomed and unresolved K-line doublet spectra with a peak at 766.5 nm and 769.9 nm respectively. The lower K-line at 766.5 nm will be absorbed at an increased range as described in section IV. Figure 18(b) is a zoomed ASD spectra of the fire taken at different instances during the flaming phase of the fire. Figure 18(c) is the complete ASD spectra of the fire from 350 nm to 2500 nm taken at various instances during fire progression. A small step at 1000 nm, is a measurement artifact of the ASD, which switches from one internal spectrograph to another at this wavelength.

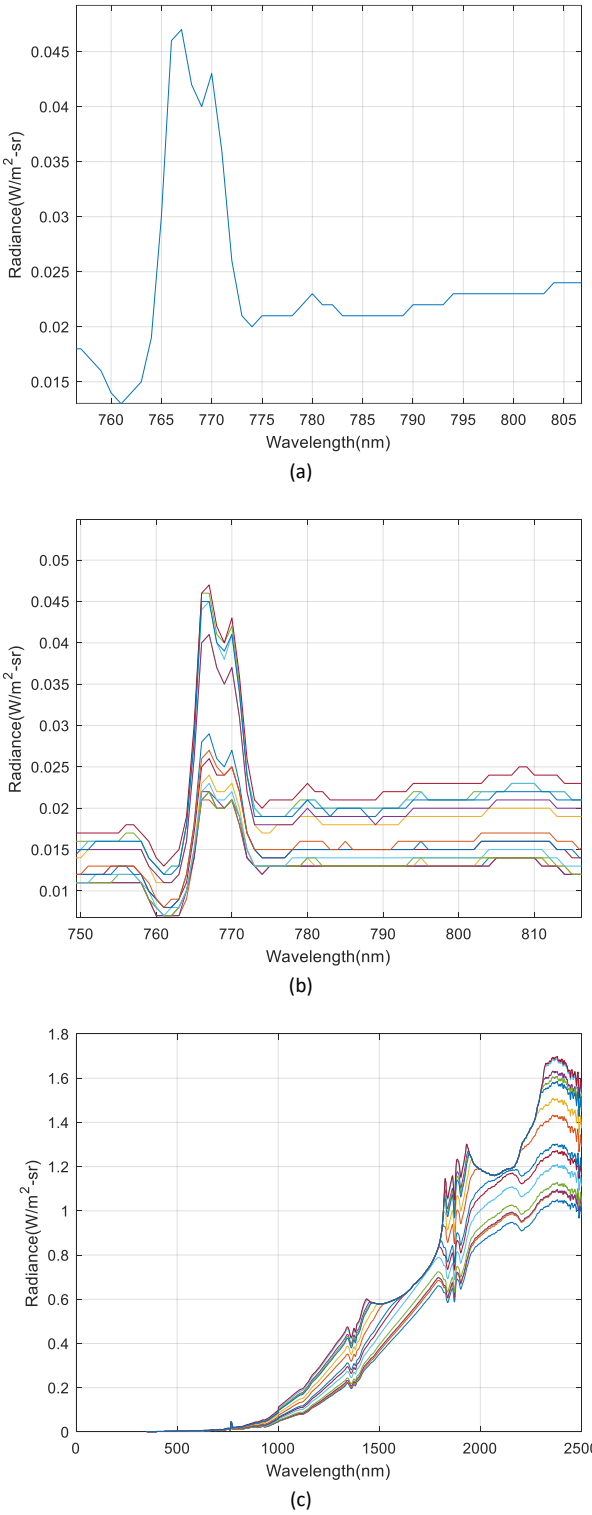

Figure 18: ASD spectral data with NIR-zoomed K-line unresolved doublet (a), zoomed spectra captured at different instances (b), and (c), the ASD spectra from 350nm to 2500nm. The Figure shows the spectral radiance of the fire within the NIR region and the short-wave band.

VI. CONCLUSION

Small-scale fires were captured using a K-line-based fire detection sensor mounted on an unmanned aerial vehicle during a field trial at the Centurion Flying Club, Pretoria, South Africa. The imaging results present strong evidence of the K-line signature within vegetation fires detectable by compact CMOS cameras operating within the NIR spectrum. The ASD spectral measurement confirmed the elemental composition of the vegetation species with a very dominant alkali metal Potassium that is embedded on the spectrum curve. The K element emissions are released at the temperature of the fire at the combustion phase.

This study demonstrates the possibility of performing early fire detection of vegetation biomass using low-cost, higher-resolution NIR sensors integrated into unmanned aerial vehicles coupled with advanced image processing algorithms. This work is recommended as a work in progress to develop a system that will not only detect but track, and geolocate fires, enable fire progression monitoring in areas that are not easily accessible, and finally, facilitate the evolution estimates of fires in real-time.

The limitations on the current development board (RaspberryPi8) such as overheating, and inability to perform onboard processing are targeted as some of the improvements to be considered for the next version of the payload.

ACKNOWLEDGMENT

The Optronic Sensor Systems (OSS) together with all the team members involved in this work owes thanks to the Aeronautical Sciences Impact Area at the CSIR for the logistical assistance and technical inputs to the project. Also, our special thanks to the Department of Science and Innovation for their financial support and funding, for enabling this research effort, as well as UAV Industries (UAV-I) for support in UAV operations during the measurement exercise.

REFERENCES

[1] E. Magidimisha, S. Naidoo, Z. Faniso-Mnyaka, and M. Nana, "Detecting Wildfires Using Unmanned Aerial Vehicle with Near Infrared Optical Imaging Sensor", The Fifteenth International Conference on Advanced Geographic Information Systems, Applications, and Services, IARIA, 978-1-68558-079-7, 2023.

[2] Y. Liu, J. A. Stanturf, and S.L. Goodrick, "Trends in global wildfire potential in a changing climate", Forest Ecology and Management, 259(2010):685–697, 2009. http://dx.doi.org/10.1016/j.foreco.2009. 09.002 (accessed Oct. 25, 2022).

[3] R. Kelly, L. Melissa. C. Philip, E. Higuera, I. Stefanova, B. L. Brubaker, and F. Sheng Hu, "Recent burning of boreal forests exceeds fire regime limits of the past 10 000 years", Proceedings of the National Academy of Sciences, 110(32):13055–13060, 2013. http://dx.doi.org/10.1073/pnas. 1305069110 (accessed Oct. 25, 2022).

[4] P. E. Dennison, D. A. Roberts, and L. Kammer, "Wildfire Detection for Retrieving Fire Temperature from Hyperspectral Data", In ASPRS 2008 Annual Conference, vol. 1, pp. 139–146, 2008. http: //www.asprs.org/a/publications/proceedings/portland08/0015. pdf (accessed Oct. 25, 2022).

[5] S. A. Robert, M. M. Joshua, J. G. Craig, and S. Jennings, "Airborne Optical and Thermal Remote Sensing for Wildfire Detection and Monitoring", MDPI open access article, Sensors 2016.

[6] J. M. Robinson, "Fire from space: global fire evaluation using infrared remote sensing", International Journal of Remote Sensing, vol. 12, pp. 3-24, 1991.

[7] D. O. Fuller, "Satellite remote sensing of biomass burning using optical and thermal sensors", Progress in Physical Geography, vol. 24, pp. 543-561, 2000.

[8] L. B. Lentile, Z. A. Holden, A. M. Smith, M. J. Falkowski, A. T. Hudak, P. Morgan, S. A. Lewis, P. E. Gessler, and N. C. Benson, "Remote sensing techniques to assess active fire characteristics and post fire effects", International Journal of Wildland Fire, vol. 15, pp. 319-345, 2006.

[9] P. J. Thomas and O. Nixon, "Near-infrared forest fire detection concept", Applied Optics, vol. 32, pp. 5348-5355, 1993.

[10] Z. Wang, "Modelling Wildland Fire Radiance in Synthetic Remote Sensing Scenes", PhD thesis, 2007.

[11] E. Magidimisha and D. Griffiths, "Remote optical observations of actively burning biomass fires using potassium line emission", Proceedings of the SPIE, vol. 10036, pp. 331-336, 2016.

[12] A. Stefania, J. Martin, B. Wooster, and A. Piscini, "Multi-resolution spectral analysis of wildfire potassium emission signatures using laboratory, airborne and spaceborne remote sensing", Remote Sensing of Environment, vol. 115, pp. 1811–1823, 2011.

[13] R. S. Allison, A. J. M. Johnston, G. Craig, and S. Jennings, "Airborne Optical and Thermal Remote Sensing for Wildfire Detection and Monitoring", Sensors, 2016.

[14] C. Yuan, Z. Liu, and Y. Zhang, "Vision-based Forest Fire Detection in Aerial Images for Firefighting Using UAVs", Proceedings of 2016 International Conference on Unmanned Aircraft Systems (ICUAS), Arlington VA, USA, 7-10 June 2016.

[15] S. Sudhakar, V. Vijayakumar, C. S. Kumar, V. Priya, L. Ravi, and V. Subramaniya, "Unmanned Aerial Vehicle (UAV) based Forest Fire Detection and monitoring for reducing false alarms in forest-fires", Comput. Commun, vol. 149, pp. 1–16, 2020.

[16] Y. Chen, Y. Zhang, J. Xin, Y. Yi, D. Liu, and H. Liu, "A UAV-based Forest Fire Detection Algorithm Using Convolutional Neural Network", Proceedings of the 37th IEEE Chinese Control Conference, Wuhan, China, 25–27 July, pp. 10305–10310, 2018.

[17] A. Vodacek, R. L. Kremens, A. J. Fordham, S. C. Vangorden, D. Luisi, J.R. Shott, and D. J. Latham, "Remote optical detection of biomass burning using a potassium emission signature", International Journal of Remote Sensing, 23(3), pp. 2721 - 2726, 2002.

[18] Nist Atomic Spectral Database. URL.http://Physics.nist.gov, 2001 (accessed Sep. 21, 2023).

[19] S. Amici, M. J. Wooster, and A. Piscini, "Multi-resolution spectral analysis of wildfire potassium emission signatures using laboratory, airborne and spaceborne remote sensing", Remote Sensing of Environment, vol. 115, no. 8, pp. 1811-1823, Aug. 2011.

[20] D. Latham, "Near-infrared spectral lines in natural fires", Proceedings of the III International Conference on Forest Fire Research/14th Conference on Fire and Forest Meteorology, pp. 513–515, 1998.

[21] F. Khan, Z. Xu, J. Sun, F. M. Khan, A. Ahmed, and Y. Zhao, "Recent Advances in Sensors for Fire Detection," *Sensors*, vol.

22, no. 9, pp. 3310 – 3333, Apr. 2022, doi: 10.3390/s22093310.

[22] "*OpenCV Tutorial Optical Flow"*, docs.opencv.org. https://docs.opencv.org/4.5.1/d4/dee/tutorial_optical_flow.html (accessed Apr. 4, 2023).

[23] A. E. Ononye, A. Vodacek, and R. Kremens, "Fire temperature retrieval using constrained spectral unmixing and emissivity estimation, Algorithms and Technologies for Multispectral, Hyperspectral, and Ultraspectral Imagery", XI 5806, pp. 352 – 360, [doi: 10.1117/12.603440], 2005.

[24] J. Shi and C. Tomasi, "Good features to track", Proceedings of IEEE Conference on Computer Vision and Pattern Recognition, pp. 593–600, IEEE, June 1994.

[25] "*OpenCV Camera Calibration and 3D Reconstruction"*, docs.opencv.org. https://docs.opencv.org/3.4/d9/d0c/group__calib3d.html#ga4abc2ece9fab9398f2e560d53c8c9780 (accessed Apr. 4, 2023).

[26] M. Zuliani, "Ransac for dummies with examples using the ransac toolbox for matlab & octave and more", 2014.

[27] "*OpenCV SimpleBlobDetector Class Reference",* docs.opencv.orghttps://docs.opencv.org/4.x/d0/d7a/classcv_1_1SimpleBlobDetector.html (accessed Apr. 4, 2023).

[28] R. W. B. Pearse and A. G. Gaydon, The identification of Molecular Spectra (London: Chapman and Hall), 1976.